

HPHT growth and x-ray characterization of high-quality type IIa diamond

This article has been downloaded from IOPscience. Please scroll down to see the full text article.

2009 J. Phys.: Condens. Matter 21 364224

(<http://iopscience.iop.org/0953-8984/21/36/364224>)

View [the table of contents for this issue](#), or go to the [journal homepage](#) for more

Download details:

IP Address: 129.252.86.83

The article was downloaded on 30/05/2010 at 04:58

Please note that [terms and conditions apply](#).

HPHT growth and x-ray characterization of high-quality type IIa diamond

R C Burns^{1,7}, A I Chumakov², S H Connell³, D Dube³,
H P Godfried^{4,8}, J O Hansen^{1,9}, J Härtwig², J Hoszowska²,
F Masiello², L Mkhonza⁵, M Rebak³, A Rommevaux², R Setshedi⁶
and P Van Vaerenbergh²

¹ Element Six Technologies, Booyens Reserve Road, Theta, Johannesburg, South Africa

² European Synchrotron Radiation Facility, BP 220, F-38043 Grenoble, Cedex, France

³ Physics Department, University of Johannesburg, South Africa

⁴ Element Six BV, PO Box 119, 5430 AC Cuijk, The Netherlands

⁵ iThemba LABS (Gauteng), Johannesburg, South Africa

⁶ Foundation Department, Cape Peninsula University of Technology, South Africa

E-mail: scrdochansen@gmail.com

Received 5 April 2009, in final form 30 July 2009

Published 19 August 2009

Online at stacks.iop.org/JPhysCM/21/364224

Abstract

The trend in synchrotron radiation (x-rays) is towards higher brilliance. This may lead to a very high power density, of the order of hundreds of watts per square millimetre at the x-ray optical elements. These elements are, typically, windows, polarizers, filters and monochromators. The preferred material for Bragg diffracting optical elements at present is silicon, which can be grown to a very high crystal perfection and workable size as well as rather easily processed to the required surface quality. This allows x-ray optical elements to be built with a sufficient degree of lattice perfection and crystal processing that they may preserve transversal coherence in the x-ray beam. This is important for the new techniques which include phase-sensitive imaging experiments like holo-tomography, x-ray photon correlation spectroscopy, coherent diffraction imaging and nanofocusing. Diamond has a lower absorption coefficient than silicon, a better thermal conductivity and lower thermal expansion coefficient which would make it the preferred material if the crystal perfection (bulk and surface) could be improved. Synthetic HPHT-grown (high pressure, high temperature) type Ib material can readily be produced in the necessary sizes of 4–8 mm square and with a nitrogen content of typically a few hundred parts per million. This material has applications in the less demanding roles such as phase plates: however, in a coherence-preserving beamline, where all elements must be of the same high quality, its quality is far from sufficient. Advances in HPHT synthesis methods have allowed the growth of type IIa diamond crystals of the same size as type Ib, but with substantially lower nitrogen content. Characterization of this high purity type IIa material has been carried out with the result that the crystalline (bulk) perfection of some of the HPHT-grown materials is approaching the quality required for the more demanding applications such as imaging applications and imaging applications with coherence preservation. The targets for further development of the type IIa diamond are size, crystal perfection, as measured by the techniques of white beam and monochromatic x-ray diffraction imaging (historically called x-ray topography), and also surface quality. Diamond plates extracted from the cubic growth sector furthest from the seed of the new low strain material produces no measurable broadening of the x-ray rocking curve width. One measures essentially the crystal reflectivity as defined by the intrinsic reflectivity curve (Darwin curve) width of a perfect crystal. In these cases the more sensitive technique of plane wave topography has been used to establish a local upper limit of the strain at the level of an ‘effective misorientation’ of 10^{-7} rad.

(Some figures in this article are in colour only in the electronic version)

1. X-ray optics and monochromator crystals

The crystal diamond has a significant place in the history of crystallography, along with sodium chloride, because it was

⁷ Present address: Element Six, Element Six Road, Nuffield, South Africa.

⁸ Present address: ASML Netherlands B.V. Veldhoven, The Netherlands.

⁹ Present address: Hansen Future Materials, South Africa.

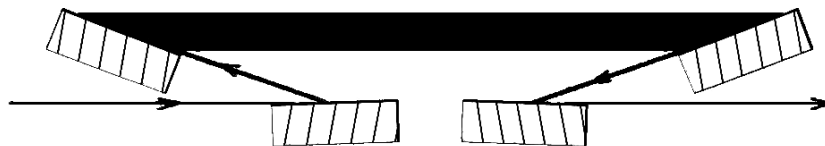


Figure 1. An ultra-high-resolution x-ray crystal monochromator providing a $120 \mu\text{eV}$ bandwidth at 14.41 keV from [2].

one of the first crystals to be studied by the father and son team of W L and W H Bragg in the development of their theory of x-ray diffraction by the lattice planes in crystals [1]. These authors commented at that time (1913) on the high transparency of diamond to x-rays, by comparison with other crystals, a property that appeared through a systematic error when analysing higher-order reflections. X-ray optical elements such as monochromators are based on the Bragg law $\lambda = 2d_{hkl} \sin \theta_B$, where λ is the wavelength of the diffracted beam, d_{hkl} the lattice plane spacing used for the given crystal reflection hkl (hkl being the Laue indices) and θ_B is the Bragg angle for this reflection. For x-rays with an incident angle close to the Bragg angle θ_B , and for the reflection or Bragg geometry, the efficiency for diffraction from the crystal can be nearly unity (with small effects from polarization, absorption and crystal quality). The range of angles over which the diffraction yield remains high (the width of the reflectivity curve) depends on the x-ray energy (or wavelength), the crystal quality, unit cell volume and the particular planes involved in the diffraction, and for highly perfect crystals this angular range is of the order of arc seconds. Silicon is the material most often used in synchrotrons for Bragg diffracting x-ray optical elements. This is because of its relatively easily obtained extremely high crystal perfection, essentially straightforward processing, large range of sample sizes and also its lifetime in the harsh conditions of a synchrotron x-ray beam. Different crystal reflections may be used to access different angular and energy acceptance ranges, but the 111 reflection is used most often. The energy range for a specific experimental station depends on the particular experimental techniques deployed. Often it is in the range between 6 and 60 keV for a high energy synchrotron like the European Synchrotron Radiation Facility (ESRF) in Grenoble, France. However, lower as well as higher energies are also exploited. Sets of monochromator crystals are normally used together in a variety of configurations, which further optimize the collimation and energy spread of the resulting x-ray beam. The Bragg diffraction process thus not only collimates an x-ray beam but also acts as an efficient energy filter or monochromator. A double-crystal set-up is most often used at synchrotrons. For very high energy resolution more complex set-ups (such as in figure 1) are used and a resolution $\Delta E/E$ of the order of 10^{-8} may be reached [2].

The most important trend in synchrotron-radiation-based x-ray sources is towards higher brilliance, i.e. more photons, out of smaller optical source sizes, in smaller solid angles and shorter pulses. This may lead to a very high power density, of the order of hundreds of watts per square millimetre at the x-ray optical elements. These elements are, typically, windows, polarizers, filters and monochromators.

A description of these is given below. The elements which are the first to be encountered by the x-ray beam and which are most likely to suffer from the high power density are the window(s) and filter(s) that may be present between source and monochromator (but may be absent in windowless vacuum beamlines) and, above all, the first monochromator crystal (normally in a double-crystal set-up often cooled with liquid nitrogen).

Silicon can be grown to a sufficiently high degree of crystal perfection and be processed with such a high quality that it is possible to build x-ray optical elements that preserve transversal coherence of the x-ray beam. This is important for the modern techniques/applications like phase-sensitive imaging experiments such as holo-tomography, x-ray photon correlation spectroscopy or coherent diffraction imaging, but also for ultimate focusing in the nanometre range. Considering the trend towards higher brilliance with the resulting problems caused by high power densities, diamond would be the preferred material if the crystal perfection (bulk and surface) could be improved [3].

2. The properties of diamond relevant to x-ray optical elements

Diamond-based elements provide several very advantageous properties. One is the low x-ray absorption of diamond, which arises because its atomic number is very low and consequently so is the electron density (see table 1). The low linear x-ray absorption coefficient (by comparison with silicon) makes it possible to 'reflect' (more exactly they are diffracted) x-rays by the monochromator (if used in the reflection or Bragg case) or to transmit x-rays through the filters and the monochromator or beamsplitter crystals, the latter to be used in transmission or Laue geometry (the Bragg case is also used), without excessive heating. But over and above this, diamond has a superior thermal conductivity and a smaller thermal expansion coefficient in addition to this low absorption, so that the energy dissipated in the optical element should be conducted away to the support mechanism relatively easily, creating only limited thermal deformation. The resulting x-ray beam deformations, due to the heat load, are expected to be up to 400 times less than in silicon at room temperature. This could lead to a simple water cooling design in all or most cases. The time structure of the beams emitted from the modern x-ray sources is also important, as these beams are pulsed with the pulse length being very short. For example, for the free-electron lasers (FELs), the pulse length is of the order of femtoseconds, which is an extreme case. The thermal load is delivered with high peak power in very short time intervals. In diamond, the thermal conductivity is mediated by the phononic system,

Table 1. Properties of importance for x-ray applications of four materials (see [4, 5]).

Material	Be	C (Diamond)	Si	Ge
Atomic number Z	4	6	14	32
Debye temperature T_d (K)	1188	1860	532	293
Absorption coefficient, μ at 8 keV (cm^{-1})	1.7	14	143	350
Thermal conductivity, κ , at 297 K ($\text{W cm}^{-1} \text{K}^{-1}$)	2.0	Type I: 5–18 Type IIa: 20–25 Isotopically pure: 35 Polycrystalline: 4–20	1.5	0.64
Thermal conductivity, κ , at low temperature ($\text{W cm}^{-1} \text{K}^{-1}$)		Ia: 20–40 (80 K) IIa: 150 (80 K) 99.9% ^{12}C : 410 (104 K) [5]	Nat 15 Isotopically pure: 20 [6]	3.25 (80 K) 2.32 (100 K)
Thermal expansion coefficient, α at 297 K (10^{-6}K^{-1})	11	1	2.4	5.6
Figure of merit, $100 \times \kappa/\mu\alpha$ at 297 K (MW)	11	36–250	0.44	0.03

which has a very fast response time in comparison to other materials.

Table 1 summarizes physical properties of importance for x-ray optical applications for the candidate materials beryllium, diamond, silicon and germanium. A figure of merit is presented in the last row of the table, which favours a weak absorption of x-rays, a very high heat conductivity and a small thermal expansion, and diamond is seen to excel here,

Three issues impede the success of diamond as an x-ray optical element: crystal perfection, size and processing technologies. These are now being addressed.

3. Selection of type IIa diamond

Natural diamond that has been grown from the minerals found within the lithosphere tends to take up inclusions of these minerals and also rather a surprising level of nitrogen with concentrations of 4–2800 parts per million by mass [7]. The nitrogen could be sedimentary nitrogen that has been subducted as part of the geological process of renewal of the Earth's crust, or alternatively it could be mantle-derived [8, 9]. During geological time the nitrogen in natural diamond tends to anneal so as to form nitrogen pairs or even higher-order poly-nitrogen centres of a type which have very little absorption in the visible spectrum. For this reason natural diamond is often seen in a near-colourless crystal form. The nitrogen atoms and nitrogen clusters still have the effect of disturbing the perfection and causing strain in the crystal. A small percentage of natural diamonds, probably not more than two per cent, has a sufficiently low nitrogen content of less than one part per million and these crystals have been classified as (natural) type IIa. In the case of x-ray optical elements, especially for monochromators, it is not only the presence of substitutional nitrogen that is significant, but also its inhomogeneous concentration within the crystal. This is manifested firstly by growth sectors with different average impurity concentration, which creates strain fields at the growth sector boundaries, and secondly by growth striations, the inhomogeneous concentration then being within

a growth sector and their resulting strain fields. Diamond samples showing the lowest strain have both very low defect concentrations as well as a very uniform distribution of the residual impurities. The relative concentration fluctuation is less important when the absolute average concentration is lower. In particular, the average nitrogen concentration should be not much higher than 10 parts per billion (see equation (1) below). Stacking faults, dislocations, precipitates and inclusions are the most undesired individual crystal defects. All the above-mentioned defects and inhomogeneities lead to strong long-range strain fields or to large imperfect regions which have the effect of producing inhomogeneities in the diffracted x-ray beams. During years of careful study, zones of natural crystals have been found which exhibit relatively good perfection of crystallinity and low strain [10], but the great majority of natural crystals are not suitable for use in applications such as monochromators.

Synthetic diamond that has been grown by the HPHT method usually has a yellow colour, shading into brown in extreme cases, because of the presence of a few tens to a few hundreds of parts per million (ppm) of nitrogen at single substitutional sites (known as the P1 centre) [11]. The nitrogen is thought to be derived from both the atmospheric air in the pore space in the materials of the synthesis capsule, and also impurity nitrogen in the solvent catalyst metals. This type of synthetic diamond is called type Ib and has been prepared for use in monochromator plates in the past. The nitrogen present in the metallic solvent (sometimes called a solvent catalyst) that is used to grow diamond crystals at HPHT has some beneficial effects on the growth processes. Principally these are the achievement of a higher growth rate without the inclusion of solvent droplets in the crystal and suppression of minor crystal growth sectors such as (110) and (311). Growth sectors are regions in the crystal, normally radiating outward from the seed, which were replaced by the growth of a single, specific crystal face, for instance (111), the octahedral face. They are best seen by ultraviolet- or cathodo-luminescence imaging of a cross section of the grown crystal, as shown in figure 2.

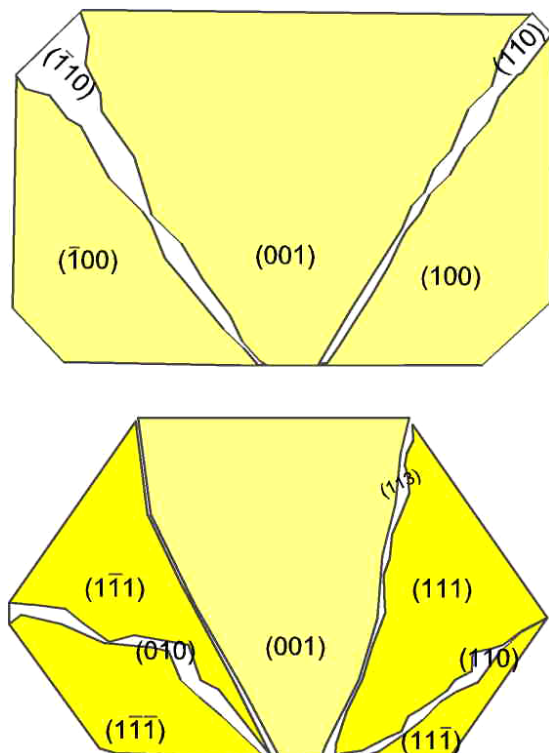


Figure 2. Growth sectors seen most frequently in the growth of near-cubic (top) and cubo-octahedral (bottom) HPHT diamond crystals of type Ib. The levels of nitrogen impurity are indicated qualitatively by the depth of the yellow colour (available in the online version), with the concentration decreasing the growth sectors in the order $\{111\} > \{100\} > \{113\} > \{110\}$.

Growth sectors can be differentiated because the uptake of impurities, most especially nitrogen, is different in the differing growth sectors. By sawing a plate from a grown crystal, in the (010) or (110) direction, polishing the plate and viewing under UV illumination, it is possible to develop images of the growth sectors. There may also be a variation of the nitrogen concentration within a growth sector, if the physical conditions change during growth. This would then lead to striations within a sector.

The lattice constant of diamond increases with increasing nitrogen content because of the relaxation of the inter-atomic bonds caused by the additional electron which is introduced by each nitrogen atom. Nitrogen has one electron more than carbon and the additional electron occupies an anti-bonding orbital. Characteristic strain fields are created at the boundary of the two growth sectors with different nitrogen concentrations. This is considered to arise from the coherent dislocation-free joining of the lattice so that the lattice parameter difference is accommodated by elastic strain only, with no compensation by misfit dislocations. Those strain fields related to the growth sector boundaries may be easily characterized by x-ray topography (see below). This also concerns concentration fluctuations within individual growth sectors, called growth striations. The lattice parameter has been measured [12–14] for its correlation with infrared absorption due to the substitutional nitrogen concentration. The infrared absorption coefficient's proportionality to the

substitutional nitrogen concentration has undergone several revisions [15–17] and aspects of this discussion are commented on [18, 19]. Considering all this, the resulting relation indicating the dependence of the dilatation of the diamond lattice on the P1 nitrogen impurity content is revised to

$$\frac{\Delta a_0}{a_0} = (0.12 \pm 0.03) \times C_N \quad (1)$$

where C_N is the nitrogen impurity concentration expressed as an atomic fraction.

A change in the nitrogen concentration (for example, at a growth sector boundary) by 100 ppm (possible in type Ib diamonds) causes a local change of the relative lattice parameter $\Delta a_0/a_0$ of 1.2×10^{-5} . This is rather high in the context of x-ray diffraction topography (very good silicon has lattice parameter inhomogeneities $\Delta a_0/a_0$ of the order of 10^{-8}) and it is sufficient to degrade the performance in applications such as monochromators¹⁰. Examples of previous studies of lattice dilatation due to single substitutional nitrogen (equation (1) above) for nitrogen-rich type Ib diamonds may be found in [26, 27]. Hoszowska *et al* [28] have carried out the characterization of both type Ib synthetic diamond and type IIa synthetic diamond grown by the best methods available at that time (2003) and concluded that only type IIa diamond can satisfy the requirements of the x-ray optical elements for applications such as imaging and phase coherence. The study of a type Ib with well-developed sectors each containing a very low nitrogen concentration that is very uniformly distributed, shown in figure 14 below, supports this conclusion.

4. Growth of synthetic type IIa diamond

The crystal growth mechanism is based upon recrystallization under a temperature gradient [29–34]. The solvent used to grow type IIa diamond should have a high affinity for nitrogen. Alloys of iron, cobalt and getter components have been used. The getters are selected from those elements which have a stable nitride at high temperatures such as titanium, aluminium and zirconium. Combinations of relatively stronger nitride formers such as titanium or zirconium and relatively weaker nitride formers such as aluminium are found to be more effective than a single getter. The relative stability of the nitrides may be inferred from tabulations of the thermodynamic properties of the metal nitrides, sometimes presented in the form of Ellingham diagrams (see figure 3).

The presence of getter components has the effect of reducing the range of temperatures in which well-formed diamond crystals will grow. At too low a temperature there is a competing process of precipitation of carbides and resorption of the diamond crystals (see figure 4).

If the temperature of growth is too high, the rate of growth is increased to the point where the metal solvent cannot be excluded and the crystal becomes contaminated by metal inclusions.

¹⁰ The strain field of a crystal plate with an inhomogeneous distribution of impurity atoms is calculated in [20] for the isotropic case and in [21] for the anisotropic case. It was applied to the quantitative analysis of x-ray topographs of quartz in [21–25]. An application to diamond, based on a different approach, was published in [14, 18].

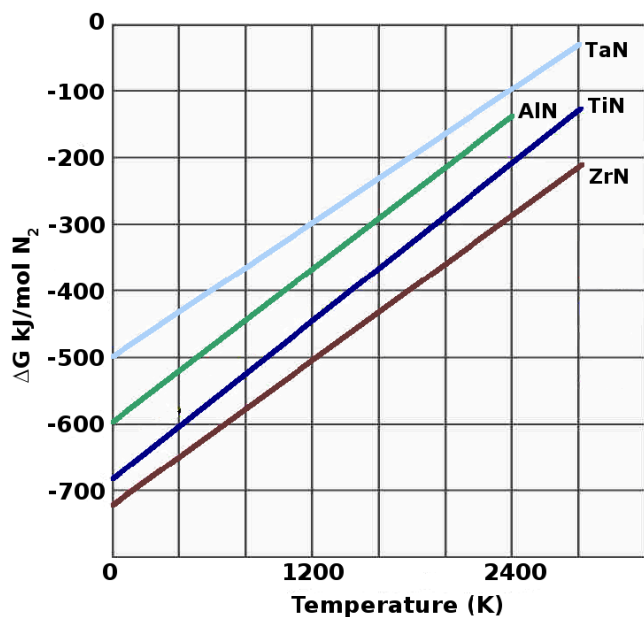


Figure 3. Stability of the nitrides of a selection of potential getter additives (more negative free energy change implies stability) from [35]. The chart is for atmospheric pressure. The lines will be displaced at high pressure: however, the order of the metals is expected to remain unaffected to first order.

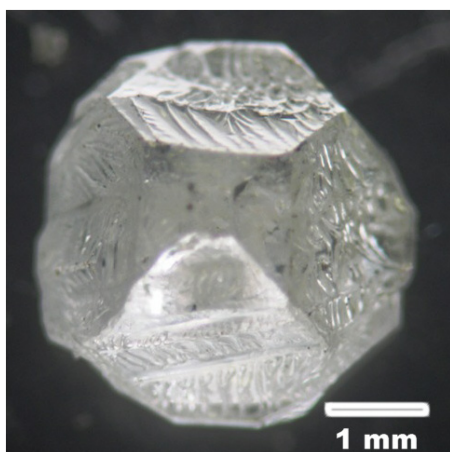


Figure 4. A type IIa diamond showing signs of too-cold growth conditions, poor facets and resorption.

The temperature range in which good crystals (see figure 5) can be grown is rather small, not more than 30° in 1350°C and for this reason an appropriate system of temperature control must be used.

In order to grow crystals of a useful size, the synthesis cycle must extend over several hundred hours. The heater elements must be able to survive for this length of time, and the high pressure, high temperature apparatus must maintain a stable pressure, in the range of 5–6 GPa during the cycle.

Because of the very low concentration of nitrogen, the type IIa crystals display a slightly different morphology than is seen generally for the case of type Ib diamonds (compare figures 2, 6 and 7).



Figure 5. A type IIa diamond grown at optimal conditions; multiple reflections of the seed interface are visible through the top face of the crystal.

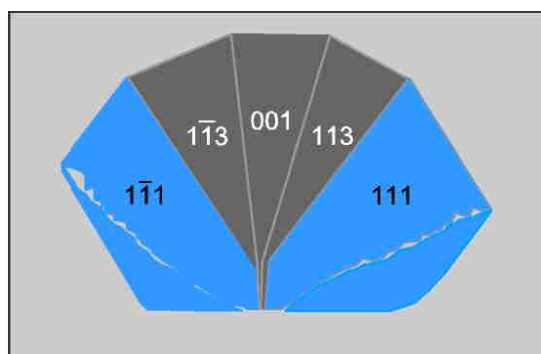


Figure 6. Growth sectors seen most frequently in the growth of HPHT diamond crystals of type IIa. The luminescence is blue. The luminescence (blue colour in the online version, lighter gray in the printed one) under ultraviolet- or cathodo-luminescent excitation is stronger in the octahedral sectors than in the other sectors which are relatively inert.

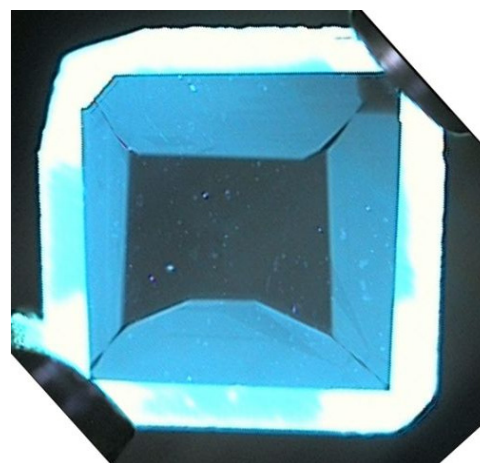
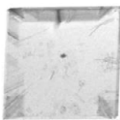
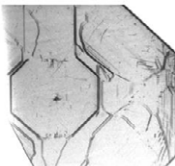
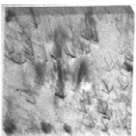
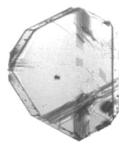


Figure 7. Ultraviolet-luminescence image of a cross section across the axis of growth of a type IIa crystal. The inner darker zones are the (001) and (113) sectors with low density of defects.

5. X-ray characterization of the diamond materials

Diamond plates of both type Ib and type IIa have been studied using the techniques of white beam and monochromatic beam x-ray diffraction topography, rocking

Table 2. Analysis of high-resolution diffraction measurements for five typical samples—an 100-oriented type IIa diamond plate from the current low strain growth series (No. 1), an older 100-oriented type Ib diamond plate for comparison and reference (No. 2), an 100-oriented CVD diamond plate (No. 3) and an 111-oriented type IIa diamond plate from an earlier growth series (No. 4). As parameters to compare the different samples with respect to their broadening due to residual strains in the bulk and due to the ‘mosaic structure’ of a thin surface layer, we show the *increases* of the rocking curve widths at 50%, 20% and 2% of the maximum intensity. For comparison the full width at half-maximum (FWHM) of the intrinsic reflectivity curves of the diamond plates for the given reflections, sample thicknesses and the energy used 14.413 keV (Darwin widths) are given. For illustration of the defect structure of the crystals, white beam topographs are added.

Diamond	No. 1 (100) IIa	No. 2 (100) Ib	No. 3 (100) CVD	No. 4 (111) IIa
White beam topographs				
Darwin widths	1.056''	1.129''	1.000''	2.954''
Δ FWHM	0.04''	0.86''	0.37''	0.43''
Δ FW20%M	0.08''	1.71''	0.74''	0.68''
Δ FW2%M	0.28''	3.25''	2.61''	11.96''

curve imaging and high-resolution x-ray diffraction (rocking curve measurements) [36–43]. Plates with a thickness of 0.5–1 mm were extracted from type IIa crystals by sawing parallel to the cubic growth face. Plate sizes of 7 mm × 7 mm can be produced from crystals of about 3 carats (600 mg).

The broadening of the experimental x-ray rocking curve (full width at half-maximum—FWHM, but also at lower levels on the wings of the rocking curve, FW20%M, FW2%M), as compared to the reflectivity curve of a perfect crystal¹¹, has often been quoted in the context of diamond as a measure of the residual strain. This is usually a more integral measurement with a rather low defect and strain sensitivity and with a lower spatial resolution, given by the footprint of the interrogating x-ray beam. Using broad beams with very low divergence (usually from synchrotrons) and deploying two-dimensional detection (CCD cameras) of the reflected x-rays, it is possible to do rocking curve mapping. It consists of taking a series of topographs with a CCD camera as a function of the angular position of the crystal (along the averaged rocking curve of the whole crystal). Parameters like the peak reflectivity, the full width at half-maximum of the rocking curve and the local Bragg angle (rocking curve position) can then be extracted numerically for each pixel of the set of topographic images to produce quantitative maps of these parameters [37]. For crystals of rather high perfection, where very slight rocking curve broadenings have to be detected, a high-resolution x-ray diffraction set-up with much reduced energy and angular spread has to be used. This is because a very narrow and well-known apparatus function is required to detect and quantitatively determine small changes of the form (in particular the increase or even no increase of the widths at different heights) for narrow reflectivity curves due to the presence of imperfections in an accurate and reliable way. The experimental and/or theoretical determination of the apparatus function is still a rather challenging problem and will not be discussed here. The rocking curve measurements were done

¹¹ The convolution of the reflectivity curve of a perfect crystal with the apparatus function of the complete experimental set-up and with a function representing the broadening of the (perfect) reflectivity curve due to the presence of crystal defects gives the experimental rocking curve.

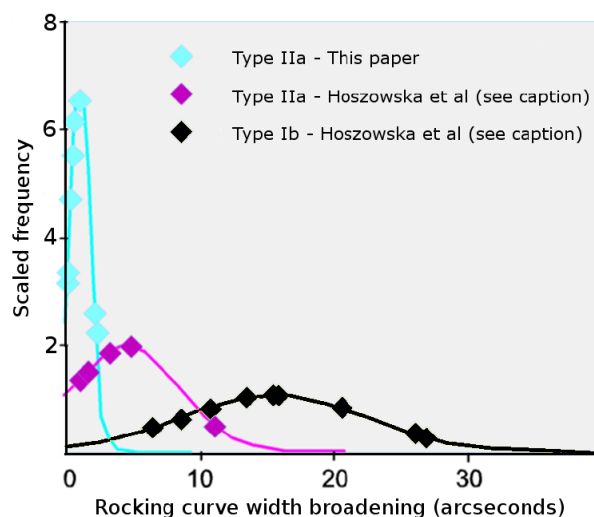


Figure 8. (a) Statistical distribution of rocking curve width broadening for three types of HPHT synthetic diamond material. Type IIa (this paper), type IIa from an earlier batch of material and type Ib, measured at ESRF by Hoszowska *et al* [38]. The points correspond to the frequency with which different values of the rocking curve width broadening occur for different points on the crystal, over the whole crystal. In some cases the data of several crystals are averaged. The current material show negligible broadening in the central region.

with a dedicated set-up at the ESRF beamline ID18, using an energy of 14.413 keV and energy spread $\Delta\lambda/\lambda$ of 10^{-8} (which corresponds to 0.0023 arcsec), an angular spread $\delta\theta$ of 0.18 arcsec and finally a (400) reflection from a (100) diamond plate.

There has been a progressive improvement in the narrowness of the rocking curve width, i.e. a reduction in the broadening of the curve, above the minimum value, for the instrument alone. This is shown schematically in figure 8 where type Ib, the earlier type IIa and the recent low strain type IIa material are compared. A comparison of examples of (rather typical) values for increases of rocking curve widths (at three levels—50%, 20% and 2% of maximum height), together with their white beam topographs for a recent 100-oriented

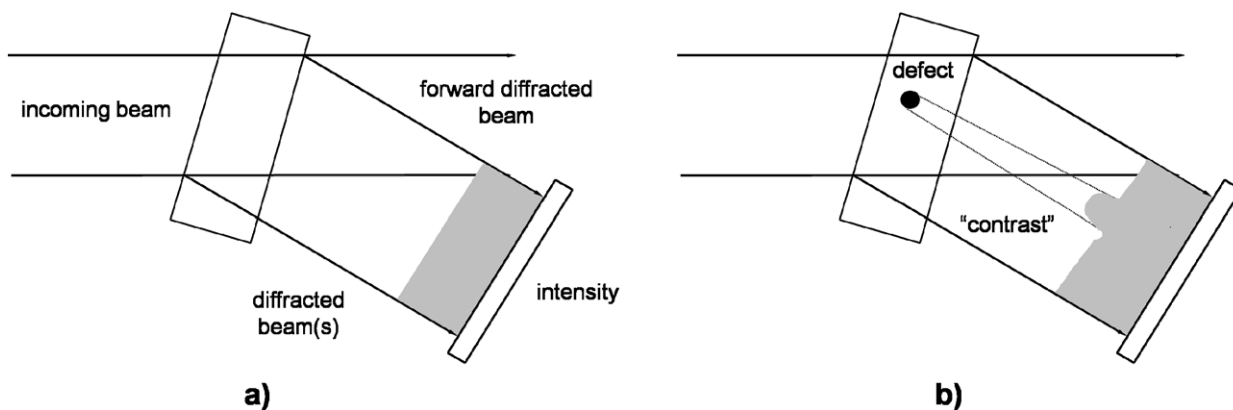


Figure 9. Basic principle of x-ray diffraction topography for an extended (homogeneous) beam. Situation for a perfect (a) and an imperfect crystal (b).

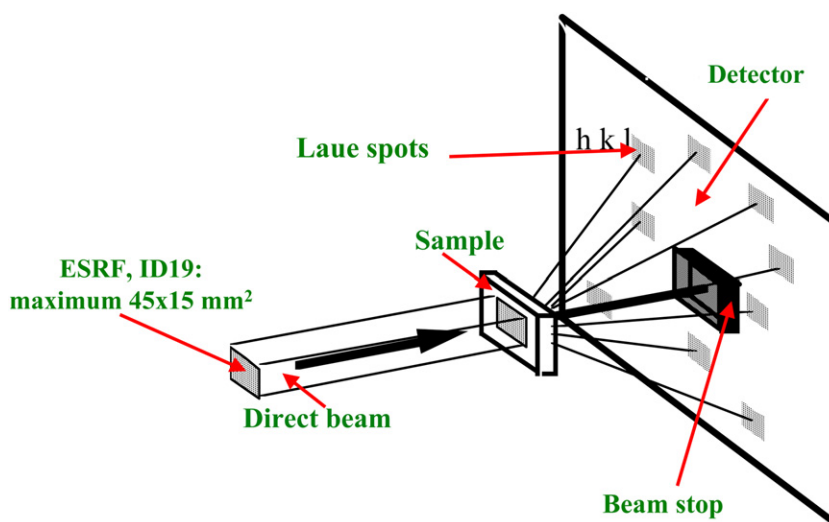


Figure 10. White beam topographic set-up.

type IIb plate, an older 100-oriented type Ia plate, an 100-oriented CVD plate and an 111-oriented type IIb plate are shown in table 2.

In the best cases for the most recent low strain type IIa material, a broadening below 0.1 arcsec of the x-ray rocking curve full width at half-maximum is observed, i.e. the crystal reflectivity is practically defined by the intrinsic reflectivity curve (Darwin curve) of a perfect crystal. Those tiny effects are probably mainly due to imperfections as the consequence of a not yet optimum surface processing and probably not to the bulk quality. This problem is under investigation. To quantify the residual strain in the case of crystals with a very low degree of imperfection, high-resolution diffraction measuring rocking curve broadening is not sensitive enough and x-ray topographical methods with high strain sensitivity and local resolution must be used.

X-ray diffraction topography is an imaging technique based on Bragg diffraction. It provides a two-dimensional intensity mapping of the beam(s) diffracted by a crystal. It is used for the visualization of defects (dislocations, stacking faults, inclusions, precipitates, growths striations, etc) that may be present in the crystal volume. More exactly, it records

the long-range strain fields associated with those defects as well as macroscopic crystal deformation (e.g. bending). This becomes possible, because these strain fields may locally affect the diffracted intensity, thereby generating ‘contrast’ (a non-homogeneous intensity distribution) in the diffracted image. In a simplified way the basic principle of x-ray topography (in the case of a large beam) is shown in figure 9. References and further details may be found, for example, in [44, 45]. Figure 10 shows a typical white beam topography set-up. Figure 11 depicts how the broad incident beam leads to several ‘Laue spots’, each being an x-ray topograph, which are each the size of the crystal studied. In this way x-ray topography is a study of the fine structure within a Laue spot which contains information about the departures from the perfect crystal structure that is, in fact, the defect structure.

Various x-ray topography techniques exist. Only a limited selection of these techniques is of importance for current practical purposes. It should be mentioned that all techniques may be used in the transmission (Laue) or in the reflection (Bragg) case.

Those of the most practical interest are techniques using extended, homogeneous incoming beams. The most

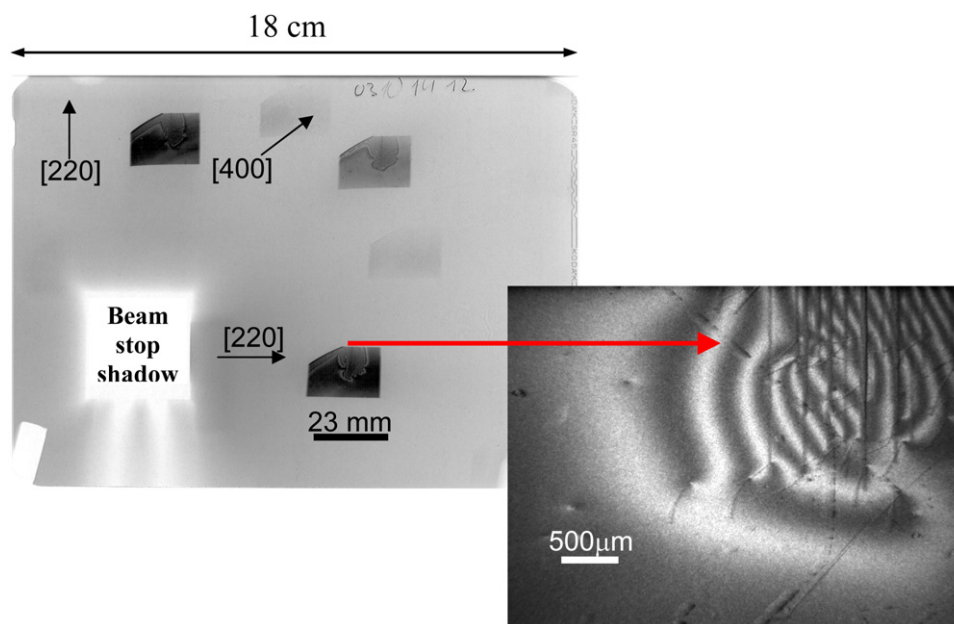


Figure 11. Example of a film with several white beam topographs (different ‘Laue spots’) and a magnified part of one topograph. Images of dislocations and scratches as well as interference fringes are visible. The sample shows a piece of a special silicon wafer (SIMOX). It was selected to have a demonstration with a large sample (centimetres rather than millimetres as is the case for diamond) for better visibility.

common technique at synchrotron sources is white beam topography. This technique uses a beam containing the continuous spectrum emitted by a bending magnet or wiggler source (in the laboratory this would be the bremsstrahlung spectrum of an x-ray tube). In this way large parts of the spectrum (and in principle also the small but not always negligible divergence range) may take part in the image formation. For this reason this technique belongs to the category of integrated wave techniques [44].

The basic arrangement for this technique is simple. It is similar to the technique used in 1912 for the first x-ray diffraction experiment (the Laue technique, used commonly, for example, for structural analysis or crystal orientation) with the main difference being that a wide, homogeneous, low divergence beam is used.

The most important advantages of white beam topography are its simplicity, that several reflections are recorded simultaneously (this allows for a semi-quantitative study of the defects exploiting contrast extinction rules), and that all crystal regions are visible simultaneously (also strongly misoriented or bent regions). The drawbacks of this technique are that it is sensitive mainly to lattice misorientations (bending). This means, for example, that growth sectors with homogeneous but different impurity concentrations may be detected only by the contrast at the growth sector boundaries (figure 12, to be compared with figure 13). Further drawbacks are the sensitivity to heat load (not significant in the case of diamond) and the limited sensitivity to very weak strains. White beam topography is a useful method for a quick evaluation of the crystal quality.

A perfect crystal would appear as a homogeneous grey topograph with practically no internal details. Under low absorption conditions (the product of the linear absorption coefficient and crystal plate thickness is smaller than one) the

defect image from a dislocation appears as a black contrast line (or double line). This is called a ‘direct image’. The larger the structure factor of the particular diffraction that is visualized (‘strong’ reflections), the narrower the dislocation images. Thus one may clearly distinguish the absence of dislocations, single dislocations or dislocations up to concentrations of roughly 10^3 – 10^5 cm $^{-3}$. The topographs are recorded on film, photographic (nuclear) plates or by CCD cameras (with a fluorescence screen and microscopy optics). The spatial resolution ranges from sub-micrometres (cameras, special holographic films) to a few micrometres (films). The use of film combines the micrometric resolution with a centimetric (or nearly infinite) field of view (something which is not possible for a camera). In addition, the resolution is often not limited by the detector resolution, but by the dynamical diffraction process itself.

In the crystals studied, dislocations originate at the seed face and grow outward. Plates extracted nearer the locus of the seed crystal appear to have more structure or detail when imaged using white beam topography. This detracts from their value as x-ray optical elements.

The limitation of white beam topography may be overcome in double-crystal or more complicated set-ups that may be roughly called monochromatic beam set-ups. However, from the image formation point of view it is important if the energy and beam divergence band of the beam impinging is larger or smaller than the related acceptance windows of the investigated crystal. In the first case it remains an integrated wave technique, but with a much narrower integration range. This allows a sensitivity to lattice tilts and lattice parameter changes, but does not reach the much higher strain sensitivities; however, the image quality is often much better. In the second case the strain sensitivity may be considerably increased using very narrow energy (and divergence) bands, in the limit that

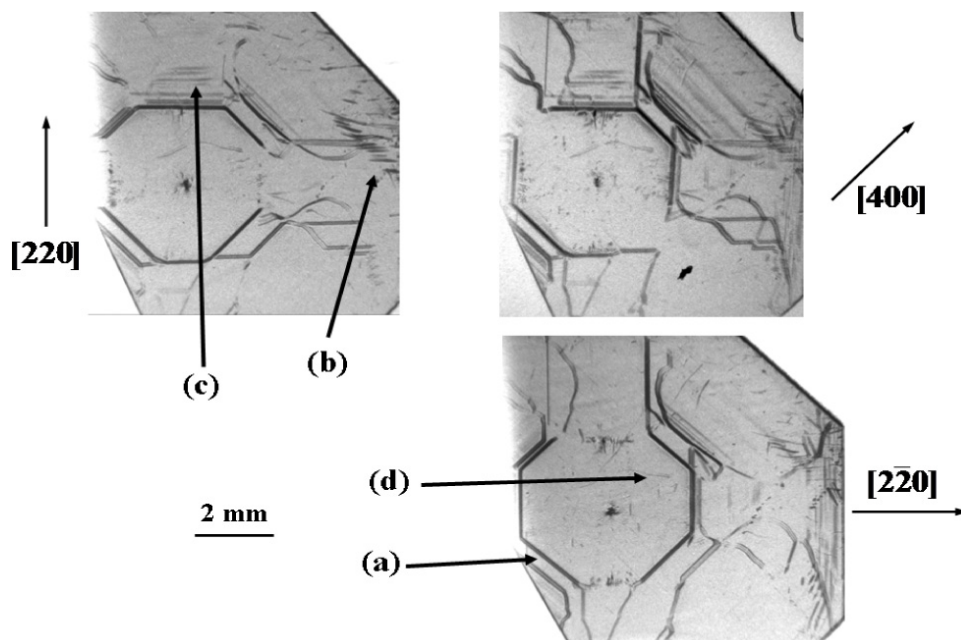


Figure 12. Example of three white beam topographs of a type Ia diamond plate with 100 orientation. All topographs were taken from one film. The main defect images visible belong to growth sector boundaries (a), few dislocations (b), growth striations (c) and scratches (d) are visible as well.

one approximates monochromatic and plane waves. Figure 13 demonstrates the different and increased strain sensitivity using the same sample as shown in figure 12. Using in addition very narrow crystal reflection curves (which results in rocking curves with very steep flanks) a direct control and increase of the sensitivity is possible when working in the steepest parts of these flanks (figure 16). In addition to this, under some rather restrictive conditions concerning the spatial variation of the strain fields, it is possible to have very simple quantitative relations between the grey level in such a topograph and the local strain [24, 44].

Figure 14 shows three examples of white beam topography of diamond plates. The first example is that of an HPHT synthetic type Ib diamond where the substitutional nitrogen impurities are present at the level of tens to hundreds of parts per million. The visible light picture has a uniform yellow colour in the nitrogen-rich (111) and (100) sectors (which show no luminescence) and is clear in the (113) and (110) sectors (which show blue luminescence). The white beam topograph shows very significant contrast, indicating a sample containing a large number of defects and lattice inhomogeneities. In particular, the boundaries between growth sectors exhibit substantial strain and bundles of dislocations are typically found perpendicular to the (100) growth sectors. This severe strain resulted in a diamond with very uniform and striation-free growth sector interiors and confirms that the more demanding x-ray applications will not be satisfied by type Ib diamond.

The ultra-pure type IIa samples studied have typically nitrogen and boron impurity concentrations in the low ppb range (determined by UV-vis spectroscopy for N and SIMS for B on representative samples). These samples exhibit excellent bulk properties which improve with distance from the seed

face. Examples of a plate extracted from a central region of the parent stone and also a plate extracted furthest from the seed is shown. The latter example has the highest lattice quality. The sample is optically clear, the central cubic sector has uniform luminescence in the UV image and no visible diffraction contrast in the white beam x-ray topograph. A model for the origin of the blue coloration in the UV-luminescence image is described in [46]. The basic phenomenon is that of broad blue band emission from donor-acceptor recombination for close pairs, as modified by the different relative concentrations of the boron acceptor and nitrogen donor within the different growth sectors. The average nitrogen and boron concentrations (each in the region of 10 ppb) are too low for sectoral changes in impurity concentrations to show up as lattice dilatation variations in the white beam x-ray topograph. Although there is also a similar blue colour (but actually a different and separated band) associated with dislocations, this is not the cause of the blue band emission we have observed. The dislocation density of this material is so low (the dislocations are individually imaged in the x-ray topography) and though there is some correlation of the dislocations with the blue band emission, this is due to their mutual correlation with different growth sectors.

The 'standard' features of the many samples are shown in figure 15 which shows a white beam topograph of another typical diamond plate originating furthest from the seed. The plate has received a final scaife polish using 100 nm diamond powder. The following features are evident and indicated on the topograph—single dislocations, stacking faults and a strain field around a microscopic (could be sub-micrometric) inclusion. The central cubic region has only a few isolated dislocations and some surface scratches. The dislocation contrast shows the well-known fine structure with

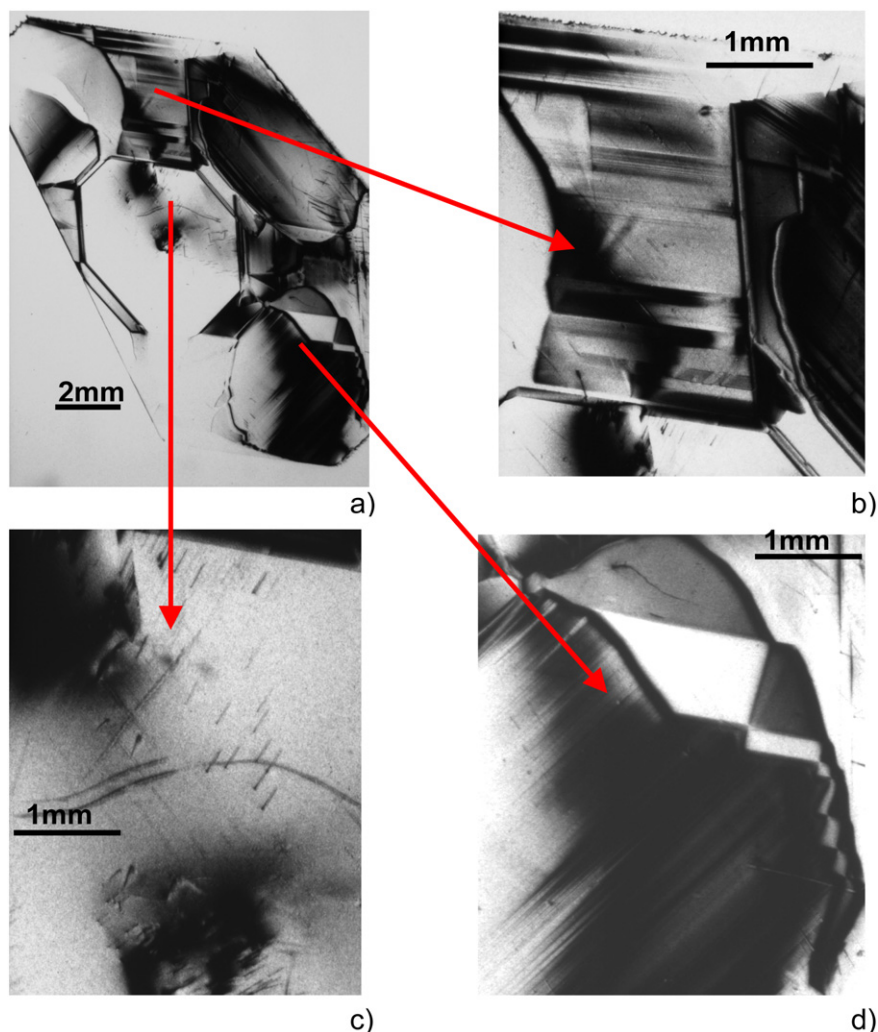


Figure 13. Example of monochromatic plane wave (approximately) topograph (a) of the same type Ia diamond plate with 100-orientation sample as in figure 12 and three magnified details ((b)–(d)). Regions that seemed to be rather homogeneous appear now very inhomogeneous. The different growth sectors and growth striations (near the arrowhead of (d)) become clearly visible, as well as dislocations and scratches (near the arrowhead of (c)). Conditions: $E = 12$ keV, non-dispersive setting, 004 reflection of the diamond sample, 444 reflection of the slightly bent Bragg-reflecting silicon monochromator.

the black line of the ‘direct image’, the white shadow of the ‘dynamical image’ and the black–white interference fringes of the ‘intermediary image’. In the wedge-shaped edge regions of the sample Pendellösung fringes (here as equal thickness fringes) are observed. The clarity of the interference patterns of the stacking fault images, the fine structure of the dislocation image, and the interference effect of the Pendellösung fringes are features that are typical of high-quality crystals [47].

As previously mentioned, the quality of the central cubic region is sufficiently high that the characterization of the sample by rocking curve measurements and possible increase of its full width at half-maximum is too insensitive.

As mentioned above, one has to employ double-crystal set-ups to obtain higher strain sensitivity. This parameter directly depends on the flank steepness of the rocking curve of the set-up. Non-dispersive arrangements, where sample and monochromator lattice parameters are identical, are the most advantageous, because they in general may have the steepest flanks. In the case of dispersive set-ups the spectral distribution

may lead to less steep flanks, but they are more flexible with respect to possible samples and reflections. Taking a topograph with a working point on the steepest part of one of the flanks of the rocking curve, the set-up has the maximal strain sensitivity. An example of such an increased sensitivity measurement in a non-dispersive set-up is displayed in figure 16. The central cubic region again survives as being essentially free of any visible contrast. Contrast in the image or non-uniform greyscale values arise due to the local effective Bragg misorientation. This is a combination of local lattice tilts and local lattice parameter changes. The contributions of these two components of the effective misorientation may be separated by repeated measurements with 90° rotations between them, as done for example in [27] and references therein. It may be quantified according to [24, 44]. For the central cubic region, essentially no strain contrast is visible. Any possible effective misorientation which may be present must be below the detection limit of the (as-used) experimental set-up of about 10^{-7} . In addition, there is also no clear contrast change at growth sector boundaries (in areas free of local

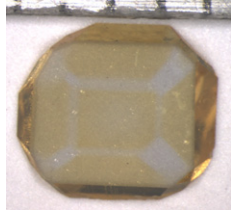
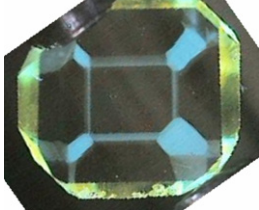
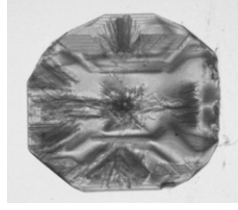
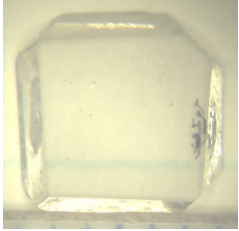
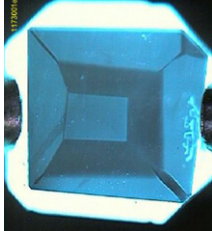
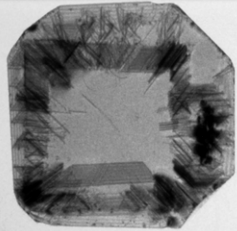
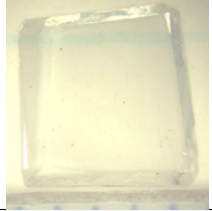
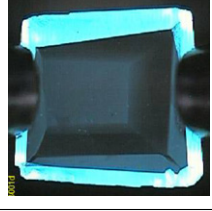
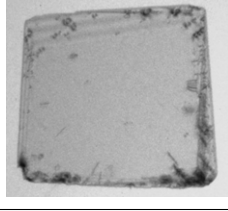
	Optical Microscopy	UV Fluorescence	White-Beam Topography
Type Ib centre plate			
Type IIa centre plate			
Type IIa top plate			

Figure 14. A set of optical and ultraviolet fluorescence images and x-ray white beam topographs. The diamond types and the origin of the plate in the parent stone are explained in the figure. (A scale in millimetres is in each optical image.)

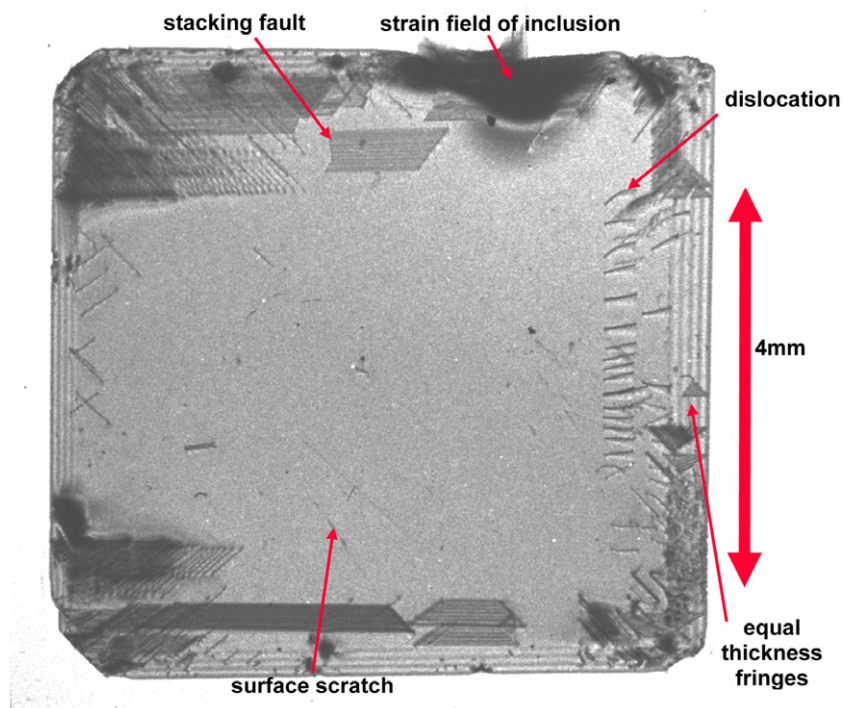


Figure 15. White beam x-ray topograph in transmission of a type IIa diamond (100) plate (450 μm thickness and sides (110) have dimensions as in the figure) with negligible diffraction contrast in the central cubic sector and some features identified in the text and in the figure.

defects). Therefore even under the more stringent conditions of non-dispersive double-crystal topography, the sectoring is not visible. This situation is consistent with an extrapolation of the Lang dilatation formula (equation (1)) down to the few ppb level and it indicates the level of purity of the HPHT samples.

6. Possible applications

The following is a summary of the type of x-ray optical elements which are candidates for application of the new type IIa diamond material.

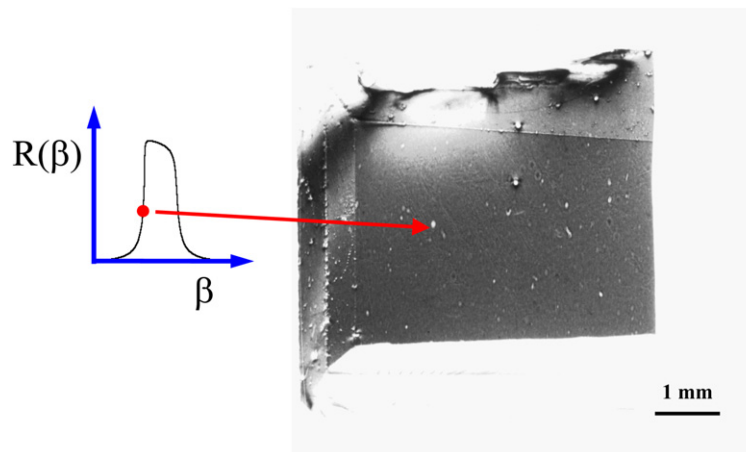


Figure 16. Quasi-monochromatic plane wave x-ray topograph in reflection geometry of a diamond with negligible diffraction contrast variation in the central cubic sector, taken at the working point on the flank of the rocking curve as shown in the inset. Same conditions as in figure 13.

- *Phase plates:* these are used to change the polarization of the x-ray beam, based on a mechanism of diffractive birefringence in the tails of the Bragg peak.
- *Lenses:* these are focusing optical elements using refractive, reflective or diffractive optics [47].
- *Monochromators:* these provide a narrow range of x-ray energies, monochromatic x-rays.
- *Beamsplitters:* these elements are also monochromators. They allow for multiple uses of one x-ray beam, by extracting successive different monochromatic beams from a wide x-ray spectrum.

Diamond is also used in the roles of windows and filters:

- *Windows:* these act as a transparent gas-tight seal between the high vacuum within the synchrotron vacuum tube, where the electrons are stored, and the experimental station where the x-rays are applied in a variety of experimental modes.
- *Filters:* these are used to remove certain softer energies from the beam.

These items are not discussed further here as the crystalline quality requirement is not severe at this stage and polycrystalline material may be used.

7. Quality classes

The overall requirements for quality of the crystal will vary depending upon the applications being contemplated for the beamline. It is useful to divide the range of quality requirements into four classes of increasing quality.

Class 1. Multiple sector growth is tolerable if $\Delta d/d$ is not larger than about 10^{-6} . Growth striations are tolerable if $\Delta d/d$ is not larger than about 10^{-6} . Dislocation densities must be less than 10^2 cm^{-2} . The reflectivity curve should not be more than a three arc seconds larger than the theoretical curve over the whole crystal. This can be satisfied by the better type Ib crystals (low and

homogeneous nitrogen content). Crystals from this class are suitable only if used in a counting applications (these measure counting rates, often with a very narrow beam) as filters, vacuum windows or phase plates, but not for imaging.

Class 2. Multiple sector growth is tolerable if $\Delta d/d$ is not larger than about 10^{-6} . Growth striations are tolerable if $\Delta d/d$ is not larger than about 10^{-6} . Dislocation densities must be less than 10^2 cm^{-2} . The reflectivity curve should be less than one arc second larger than the theoretical curve over the whole crystal. This can be satisfied by good type IIa crystals. Crystals from this class are suitable only if used in a counting applications as filters, vacuum windows, beamsplitters and monochromators, but not for imaging.

Class 3. Single-sector growth is required. No detectable growth striations ($\Delta d/d$ is not larger than about 10^{-7} – 10^{-8}). No dislocations. The reflectivity curve must be essentially similar to the theoretical curve over the whole crystal. This means no observable broadening of the rocking curve (0 arcsec). This can be satisfied by very good type IIa crystals. Crystals from this class are suitable for imaging applications (two-dimensional information, often obtained with a rather wide and spatially homogeneous beam), if used as beamsplitters, monochromators, filters and vacuum windows.

Class 4. Single-sector growth is required. No detectable growth striations ($\Delta d/d$ is not larger than about 10^{-7} – 10^{-8}). No dislocations. The reflectivity curve must be essentially similar to the theoretical curve over the whole crystal. This means no observable broadening of the rocking curve (0 arcsec). Best possible surface finish (surface roughness of the order of or less than 3 \AA). Surface miscut less than a few hundredths of a degree. This is expected to be satisfied by good type IIa crystals with an appropriate surface processing. Crystals from this class are suitable for imaging applications with coherence preservation, if used as beamsplitters, monochromators, filters and vacuum windows.

8. Summary and conclusions

The imperative to develop synthesis and processing techniques for diamond to the standards required for x-ray optical elements appropriate for both current and future synchrotron-generated x-ray beamlines has been discussed. A study has been made of conventional type Ib HPHT material, as well as a very low strain type IIa HPHT material. The synthesis conditions of this new material have been discussed. Among other factors, the growth rate must be reduced by comparison with the growth of type Ib diamond, so as to ensure growth of high-quality crystals. At this time, sizes of 7 mm square can be produced in the (100) orientation.

The results of the x-ray characterization for the type Ib material confirm that homogeneity of residual elemental impurities is not sufficient to ensure a strain-free lattice, even within growth sectors. The residual impurity concentration should be significantly lower than the Lang dilatation formula (equations (1)) extrapolated to the very low concentration limit of a few ppb to achieve residual strains lower than 10^{-7} (as expressed by an effective misorientation). The study of the low strain type IIa material have indicated that the central cubic growth sector of the plate extracted furthest from the seed face is of a quality that rocking curve measurements are not able to quantify the residual strain. Instead, the more sensitive technique of plane wave topography must be deployed. Here it was found that the residual strain could not yet be quantified. Only an upper limit on the residual strain for this region of 10^{-7} has been estimated. There are very few or sometimes even no dislocations remaining in this central cubic region. Surface scratches are easily observed. The surrounding growth sectors may still have dislocations and stacking faults, and occasionally, strain fields surrounding a microscopic metallic inclusion.

It was found to be useful to identify four classes of diamond crystal quality, in order to match the requirements of different measurement modalities in beamlines with a range of x-ray optical elements. The two lower classes can be met with type Ib and type IIa materials which are already available. Already there have, in fact, also been several examples of material where the next higher quality (Class 3) could be satisfied. This is the central cubic region in a (100) plate extracted furthest from the seed face of a low strain type IIa HPHT synthetic diamond. It is envisaged that both improvements in growth technology and also surface processing will be necessary in order to attain the levels of perfection required for the highest quality material (Class 4) required. In all cases, larger crystals are also a target.

Acknowledgments

The authors would like to acknowledge the assistance of Francis Tshisikhawe and Tim Addison for their contribution to the growth of the type IIa materials. The support and encouragement of the management of the Technologies Division of Element Six is greatly appreciated. SHC, DD, LM and RS acknowledge support from the South African NRF and the THRIP programme. JH, PVV, SHC, DD, FM,

LM and RS acknowledge support from the Joint France/South Africa Science and Technology Agreement—Research Grant (PROTEA) 05 ARS F25/SA.

References

- [1] Bragg W L and Bragg W H 1913 *Proc. R. Soc. A* **89** 277–90
- [2] Yabashi M, Tamasaku K, Kikuta S and Ishikawa T 2001 *Rev. Sci. Instrum.* **72** 4080–3
- [3] Grübel G, Abernathy D, Vignaud G, Sanchez del Rio M and Freund A K 1996 *Rev. Sci. Instrum.* **67/9** 1–4
- [4] See for example, Field J (ed) 1992 *The Properties of Natural and Synthetic Diamond* (London: Academic) pp 216–20
- [5] Wei L, Kuo P K, Thomas R L, Anthony T R and Banholzer W F 1993 *Phys. Rev. Lett.* **70** 3764–9
- [6] Kremer R K, Graf K, Cardona M, Devyatikh G G, Gusev A V, Gibin A M, Inyushkin A V, Taldenkov A N and Pohl H-J 2004 *Solid State Commun.* **131** 499–503
- [7] Sellschop J P F 1979 *The Properties of Diamond* ed J E Field (New York: Academic) chapter 4, Table 4.1
- [8] Eldridge C S *et al* 1991 *Nature* **353** 649–53
- [9] Cartigny P 2005 *Elements* **1** 79–84
- [10] Lang A R 1992 *The Properties of Natural and Synthetic Diamond* ed J Field (London: Academic) pp 216–20
- [11] Cox A, Newton M E and Baker J M 1994 *J. Phys.: Condens. Matter* **6** 551–63
- [12] Kaiser W and Bond W L 1959 *Phys. Rev.* **115** 857–63
- [13] Lang A R, Moore M, Makepeace A P W, Wierzchowski W and Welbourn C M 1991 *Phil. Trans. R. Soc. A* **337** 497–520
- [14] Arridge R G C, Lang A R and Makepeace A P W 2002 *Proc. R. Soc. A* **458** 2623–43
- [15] Chrenko R, Strong H M and Tuft R E 1971 *Phil. Mag.* **23** 313–8
- [16] Woods G S, van Wyk J A and Collins A T 1990 *Phil. Mag. B* **62** 589–95
- [17] Kiflawi I, Mayer A E, Spear P M, Van Wyk J A and Woods G S 1994 *Phil. Mag. B* **69/6** 1141–7
- [18] Arridge R G C, Lang A R and Makepeace A P W 2002 *Proc. R. Soc. A* **458** 2485–521
- [19] Davies G 1999 *Physica B* **273/274** 15–23
- [20] Härtwig J 1981 *Cryst. Res. Technol.* **16** 1297–307
- [21] Härtwig J and Lerche V 2009 *Phys. Status Solidi a* **109** 79–91
- [22] Alter U, Härtwig J and Kuběna J 1985 *Czech. J. Phys. B* **35** 158–67
- [23] Härtwig J, Jäckel K-H and Lerche V 1987 *Cryst. Res. Technol.* **22** 951–9
- [24] Lerche V, Dörnfelder P and Härtwig J 1991 *Phys. Status Solidi a* **128** 269–83
- [25] Bernhardt H J, Härtwig J and Lerche V 1992 *Prog. Crystal Growth Charact.* **24** 1–51
- [26] Wierzchowski W, Moore M, Makepeace A P W and Yacoot A 1991 *J. Cryst. Growth* **114** 209
- [27] Macrander A T, Krasnicki S, Zhong Y, Maj J and Chu Y S 2005 *Appl. Phys. Lett.* **87** 194113
- [28] Hoszowska J, Freund A K, Sellschop J P F, Burns R C, Rebak M, Hall C E, Ishikawa T, Härtwig J, Boller E, Mirone A, Rommeveaux A, Guigay J-P, Hustache R and Massonat J-Y 2004 *Int. Workshop on Diamond Single Crystals for 3rd and 4th Generation X-ray Sources, ESRF Grenoble (May 2004)* ed J Härtwig see report in [48] (and also 36, 38–40)
- [29] Burns R C, Hansen J O, Spits R A, Sibanda M, Welbourn C M and Welch D L 1999 *Diamond Relat. Mater.* **8** 1433–7
- [30] Sumiya H, Toda N and Satoh S 2002 *J. Cryst. Growth* **1281** 237–9
- [31] Sumiya H, Toda N and Satoh S 2005 *SEI Tech. Rev.* **60** 10

- [32] Sumiya H and Satoh S 1996 *Diamond Relat. Mater.* **5** 1359–65
- [33] Kanda H 2000 *Braz. J. Phys.* **30/3** 482–89
- [34] Babich Y V, Feigelson B N, Fisher D, Yelisseyev A P, Nadolinny V A and Baker J M 2000 *Diamond Relat. Mater.* **9** 893–6
- [35] Darken L S and Gurry R W 1953 *Physical Chemistry of Metals* (New York: McGraw-Hill) p 370
- [36] Sellschop J P F, Connell S H, Nilen R W N, Freund A K, Hozzowska J, Detlefs C, Hustache R, Burns R C, Rebak M, Hansen J O, Welch D L and Hall C E 2000 *New Diamond Frontier Carbon Technol.* **10/5** 256–8
- [37] Lübbert D, Baumbach T, Härtwig J, Boller E and Pernot E 2000 *Nucl. Instrum. Methods B* **160** 521
- [38] Hozzowska J, Freund A K, Boller E, Sellschop J P F, Level G, Härtwig J, Burns R C, Rebak M and Baruchel J 2001 *J. Phys. D: Appl. Phys.* **34** A47–51
- [39] Freund A K, Hozzowska J, Sellschop J P F, Burns R C and Rebak M 2001 *Nucl. Instrum. Methods A* **467** 384–7
- [40] Sellschop J P F, Freund A, Hozzowska J, Connell S H, Rebak M and Burns R C 2002 *Phys. Status Solidi a* **193/3** 415–22
- [41] Tamasaku K, Ueda T, Miwa D and Ishikawa T 2005 *J. Phys. D: Appl. Phys.* **38** A61–6
- [42] Zhong Y, Krasnicki S, Macrander A T, Chu Y S and Maj J 2005 *J. Phys. D: Appl. Phys.* **38** A39–43
- [43] Zhong Y, Macrander A T, Krasnicki S, Chu Y S, Maj J, Assoufid L and Qian J 2007 *J. Phys. D: Appl. Phys.* **40** 5301–5
- [44] Bowen K D and Tanner B K 1998 *High Resolution X-Ray Diffraction and Topography* (Boca Raton, FL: CRC Press)
- [45] Härtwig J School Material on the ESRF web-page, http://www.esrf.fr/exp_facilities/ID19/homepage/DiffTopo/X-raytopography.htm
- [46] Watanabe K, Lawson S C, Isoya J, Kanda H and Sato Y 1997 *Diamond Relat. Mater.* **6** 99–106
- [47] Nohammer B *et al* 2003 *J. Physique IV* **104** 223–6
- [48] Härtwig J and Connell S H 2005 *Synchrotron Radiat. News* **18/1** 15–9